Role of zeolite content on the sorption properties of analcime-rich rocks from the Abinky Formation (Niger)

Flora Parrotin, Baptiste Dazas, Sophie Billon, Raphaël Chedozeau, Sébastien Savoye, Michaël Descostes, Emmanuel Tertre

Role of zeolite content on the sorption properties of analcime-rich rocks from the Abinky Formation (Niger)

Flora Parrotin[1,3,*], Baptiste Dazas[1], Sophie Billon[1], Raphaël Chedozeau[1], Sébastien Savoye[2], Michaël Descostes[3,4] & Emmanuel Tertre[1]

[1] IC2MP, Equipe HydrASA, UMR 7285/Université de Poitiers, 86073 Poitiers, France

[2] Université Paris-Saclay, CEA, Service de Physico-Chimie, 91191 Gif-sur-Yvette, France

[3] ORANO Mining, Environmental R&D Dpt., 92320 Chatillon, France

[4]Centre de Géosciences, MINES Paris, PSL University, 35 rue St Honoré, 77300 Fontainebleau, France

* E-mail address of the corresponding author:

Flora PARROTIN: flora.parrotin@univ-poitiers.fr

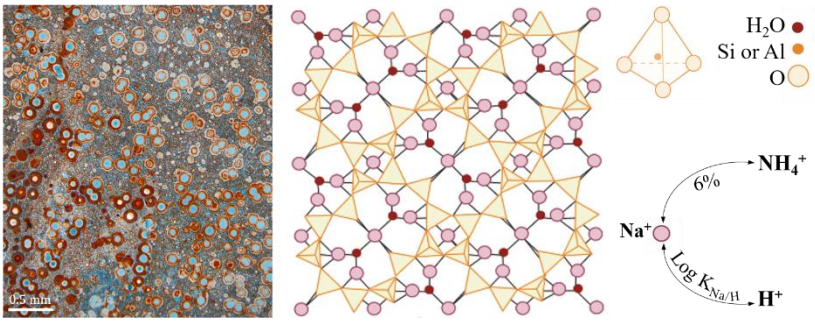

Graphical abstract

Highlights

- Validation of a method quantifying proportions of mineral and amorphous phases
- Good agreement of analcime crystal chemistry between the Rietveld method and EDS analyses
- Positive correlation between analcime content and amounts of Na^+ exchanged by NH_4^+
- Na^+/H^+ exchange is the primary H^+ consumer at the analcime/water interface at pH>3.5
- Thermodynamic model for Na^+/H^+ exchange in analcime in chloride and sulfate media

Keywords

Natural analcime-rich rocks, Rietveld refinement, Na^+/NH_4^+ and Na^+/H^+ ion exchange, dissolution.

Abstract

The Abinky formation, composed of analcimolites (*i.e.*, rocks with <70wt% analcime), underlies Tchirezrine II, which hosts the Imouraren (Niger) uranium deposit. A potential mining project is under consideration to recover U by in situ acid leaching. Analcimolites are uncommon rocks, and assessing their ion-exchange properties is the first step to understand and predict the mobility of aqueous species in these formations. The objective of this study is then to understand the link between the Cation Exchange Capacities (CEC) of analcimolites as a function of their analcime content and associated crystal chemistry. Mineral quantification was performed by Rietveld refinement constrained by local chemical analysis with scanning electron microscopy coupled with Energy Dispersive Spectrometry. CEC were obtained at neutral pH by performing NH_4^+-for-Na^+ exchange ($CEC_{Na/NH4}$), and Na^+/H^+ ion exchange experiments were performed with 4 analcimolites.

Results showed that the analcime crystal chemistry deduced from Rietveld refinement was in good agreement with that obtained from SEM analysis (1.99<Si/Al<2.53). The results showed that all samples had a positive correlation between $CEC_{Na/NH4}$ and analcime content until ~30 meq/100 g for a sample containing ~85wt%$_{Riet.}$ of analcime, and that ~6% of the total amounts of Na^+ present in the analcime could be exchanged by NH_4^+ and H^+. Based on Si and Al aqueous measurements, results showed that exchange with Na^+ is the main process consuming H^+ during Na^+/H^+ exchange when pH>3.5. These experimental data were then interpreted by considering a single site equal to the $CEC_{Na/NH4}$ value, specific for each analcimolite, and a selectivity coefficient equal to log $K_{Na/H}$=1.3 (Gaines Thomas convention) being equal for all samples investigated. Finally, these data were used to assess the role played by Na^+/H^+ exchange in the pH evolution of the pore water of an analcime-rich rock subjected to dynamic acidification.

1. Introduction

Zeolites are aluminosilicates known to have molecular sieve/guard properties related to the cage-like arrangement of the crystalline structure (Clifton, 1987; Deer et al., 2004) as well as cation exchange capacities. Due to these properties, zeolites have been used in many applications. In agriculture, zeolites are incorporated into animal feed (Pond et al., 1984; Defang and Nikishov, 2009) and in soils, they are used to promote plant development (Pond et al., 1984; Ming and Allen, 2001; Ming and Boettinger, 2001). They have also been applied for water and soil treatment (Mercer and Ames, 1978; Semmens and Seyfarth, 1978; Kalló, 2001; Komarneni and Roy, 1981; Kalita and Chelishchev, 1995), in gas separation or enrichment (Hayhurst, 1978; Kotsis et al., 1982), in construction materials (Aiello et al., 1995; Colella et al., 2001) and in biological treatments (Tsitsishvili et al., 2020).

Analcime or analcite is a natural sodium zeolite, with the theoretical formula $NaAlSi_2O_6.H_2O$, and this hydrated tectosilicate presents isomorphic substitutions of Si^{4+} by Al^{3+}, leading to a permanent negative charge in the crystalline edifice. Such charge imbalance is compensated by incorporating hydrated Na^+ atoms in the structure, enabling cationic exchange properties. Its crystal system is cubic (Ia3d) (Taylor, 1930), even though in later refinements (Calleri and Ferraris, 1964; Knowles et al., 1965; Ferraris et al., 1972; Pechar, 1989), researchers proposed up to twenty occurrences of analcime having various crystal systems and space groups (Mazzi and Galli, 1978; Hazen and Finger, 1979) with cubic, tetragonal (I41/acd or I41a) and orthorhombic (Ibca) majority. Analcime crystals can contain up to 8 wt% water trapped in their cages (Line et al., 1994), which can have sizes varying from 0.28 to 0.32 nm (Ming and Mumpton, 1989; Mimura et al., 1995). Since the cages contain water molecules (one for two silicon atoms), analcime can be used as a model system for studying water framework interactions in aluminosilicates (Line et al., 1994). Due to the

small size of its cages, no ionic sieving properties are conferred to it; it allows only molecules with diameters smaller than the size of its cages, such as H_2, He, and H_2O (Sakirci, 2016). As far as its ionic exchange properties are concerned, the cationic exchange capacity of analcime increases after heating (Barrer, 1981). Thus, some authors reported that the ion-exchange properties of synthetic analcimes subjected to heat treatment increased Na exchange capacity. They also mentioned that Na^+ could be exchanged with some cations, such as K^+, NH_4^+, Ag^+, Tl^+ and Rb^+, but not with Li^+, Cs^+, Mg^{2+}, Ca^{2+}, or Ba^{2+}, which was related to the hydrated ionic radii of these cations (Barrer and Hinds, 1953; Barrer, 1981; Dyer et al., 2004; Sakirci, 2016; Pesonen et al., 2021).

Analcime occurs in many natural environments, such as sedimentary systems (diagenesis and burial metamorphism of sediment and sedimentary rocks or marine sediment from arc-source terrains), open or closed hydrological systems (tuff in lacrustrine sediment with or without volcanic glass), deep sea sediment cavities in basaltic lava flows, hydrothermal or deuteric alteration, geothermal systems, and superficial systems such as soils and superficial deposits (Deer et al., 2004).

In northwestern Niger, significant occurrences of analcime are found from the upper Permian to Jurassic formations, which host the uranium deposit of Imouraren. This deposit is expected to be mined via both open pit mining (in the northern part) and *in situ* acid leaching (in the southern part) (called ISR for *In Situ* Recovery; IAEA, 2001). The uranium in this area is hosted in the fluvial sandstone aquifer of the Tchirezrine II formation containing analcime cement and some levels of analcime-rich rock called analcimolite. The underlying Abinky formation consists of analcimolite several tens of meters thick, with, below, the Teloua III, a sandstone aquifer containing also analcime. Analcimolite is an uncommon rock whose main mineral is analcime (generally exceeding 50%), which can occur in the form of spherules.

Few occurrences similar to Nigerien analcimolites have been described, especially in (i) the Mezosoic formation in Congo (Vanderstappen and Verbeek 1959), whose origin appears to be diagenetic with no volcanogenic material contribution, and in (ii) the Pogo Agie Member of the Chugwater Formation (High and Picard, 1965), interpreted as the result of the alteration of volcanic material in sodium-rich water. As far as the Nigerien analcimolite formation is concerned, it is the result of diagenetic processes. However, the origin of analcimes is still debated. Most authors (Pacquet, 1968, Wagani, 2007) have concluded that this mineral results from burial alteration of volcanic materials, but the evidence of pyroclastic material is too scarce in the literature (*i.e.* microscopic observations of the Abinky formation tend to indicate the absence of volcanogenic material) to conclude clearly about the origin of analcimes in this Nigerien analcimolites. Other origins, such as clay mineral transformation or direct precipitation from alkaline lake/floodplain (or pore water) are not excluded by these authors and are at least as likely conceivable than a volcanogenic origin. The column stratigraphy of the studied formations is shown in Fig. S1.

Analcime is one of the main constituents of both the Tchirezrine II and Abinky formations. However, the properties of analcimes present in natural environments were mainly acquired to address geological issues such as the effects of H_2O vapor pressure and temperature on the zeolites, the source of analcime for mining exploitation (Underdown et al., 1990; Eyde, 1993; Chipera and Bish, 2010; Sakirci, 2016; Zhu et al., 2020; Wang et al., 2022), or the origins of their formations (High and Picard, 1965; Pacquet, 1968; Hay, 1970; Valsardieu, 1971; Gall and Hyde, 1989; Remy and Ferrell, 1989; Renaut, 1993; English, 2001). However, the link between exchange properties, crystal chemistry and the proportion of analcime in these rocks remains to be established in a natural environmental context (*i.e.*, room temperature and for major cations in natural waters). Our understanding of the role played by natural analcimes in

131 the behavior of cationic elements in geological systems at room temperature (Ames, 1966) is
132 thus limited.

133 Then, prior to any potential exploitation of Tchirezrine II by ISR, reactive transport models
134 (Lagneau *et al.*, 2019; de Boissezon *et al.*, 2020; Escario *et al.*, 2023) need to be developed to
135 assess the effect of acid injection into Tchirezrine II on the reactivity of analcime and on the
136 confining properties of the Abinky formation that separates the two aquifers of Tchirezrine II
137 and Teloua II. These properties will directly depend on the hydrodynamic, mineralogical and
138 geochemical properties of this analcime-rich formation. Indeed, a good understanding of the
139 minerals involved in acid consumption, based on their solubility and sorption properties, is
140 essential for optimizing mining operations. This makes it possible to better adjust the amount
141 of acid used for treatment and thus control the composition of the aquifer water during and
142 after mining activities. In addition, zeolites, known for their ion-exchange properties, can
143 influence the mobility of many metals and trace radioelements that can be mobilized by
144 mining operations. Therefore, an evaluation of the ion-exchange properties of analcime-rich
145 rocks involving H^+ is the first step to understand and predict the consumption of protons and
146 the mobility of water and solutes in these different geological formations subjected to
147 acidification processes. Thus, the objective of this study is to understand the link between the
148 cation exchange capacities (CECs) of analcime-rich rocks as a function of (i) the analcime
149 content and (ii) the crystal chemistry of the analcime present. Mineral quantification was
150 performed by Rietveld refinement of experimental X-ray diffraction (XRD) patterns.
151 Validation of this method was assessed by comparing calculated percentages of crystalline
152 and amorphous phases with those of whole-rock. At room temperature, maximal CEC values
153 were obtained at neutral pH by performing NH_4^+-for-Na^+ exchange (CEC_{Na/NH_4}).
154 Experimental Na^+/H^+ exchange isotherms in both chloride and sulfate media were also

obtained for four samples with high analcime content to quantify Na^+/H^+ exchange capacity and the effect of aqueous speciation. Because proton consumption can occur due to both exchange and/or dissolution (Underdown et al., 1990), the prioritization of proton consumption was assessed, and Na^+/H^+ selectivity coefficient interpreting those data was obtained for both aqueous media through the use of a monosite model. Finally, the significant role of Na^+/H^+ exchange in the pH evolution of the pore water of an analcime-rich rock subjected to dynamic acidification is discussed.

2. Material and method

2.1. Natural samples and preparation

Analcime-bearing samples from the Imouraren uranium deposit (Niger) were presented first by Joulia et al. (1958), Vanderstappen and Verbeek (1959) and Millot (1963) and later studied in the works of Pacquet (1968) and Valsardieu (1971). The host formation of the uranium deposit, Tchirezrine II (Tchi2), is framed by the Abinky formation (upper Jurassic) below and the Assouas formation (lower Cretaceous) above and has an average thickness of 40 m (see stratigraphy in Fig. S1). Tchi2 is composed of arkosic sandstones with conglomerates and coarse and fine sandstones. The average mineralogical composition of these sandstones is essentially quartz, analcime, K-feldspar, albite, chlorite, and more rarely illite and calcite (Billon, 2014; Billon and Patrier, 2019). This analcime was observed as cement, analcimolitic intraclasts (Fig. S2) and analcimolitic levels over a thickness of a few meters to several dozen meters (Joulia et al., 1958; Vanderstappen and Verbeek, 1959; Millot, 1963; Pacquet, 1968; Valsardieu, 1971; Billon, 2014; Billon and Patrier, 2019). Both analcimolitic levels and intraclasts show analcimes in the form of spherules, while cement is composed of euhedral analcime. Below Tchi2 lies the Abinky formation at depths of 150-160

m in the hanging wall, which is composed of pure analcimolites and quartz-analcimolites. Due to its heterogeneity, Tchi2 can contains contrasting amounts of analcime ranging from 0 to 50wt% depending on whether it consists of sandstone facies, analcime-rich sandstone facies (rich in analcime cement or in analcimolite intraclast) or analcimolite facies. In contrast, the Abinky formation can contain 50 to 85wt% analcimes because the Abinky has some level of quartz, especially in its deepest part.

To achieve a representative sampling of the four facies (Pacquet, 1968; Billon, 2014) as well as contrasting amounts of analcime, thirty-seven samples were selected that could be classified according to 4 main facies:

- (i) The Abinky analcimolites, which is the facies at the top of the Abinky formation. These analcimolites are composed mostly of analcimes in the form of spherules aggregated by a cement of euhedral analcime and, to a lesser extent, of chlorite and iron oxides found both inside analcime spherules and in cement.
- (ii) The Abinky quartz-analcimolites, mainly located at the bottom of this formation (above the previous facies), which are quite similar to Abinky analcimolite but with additional detrital quartz.
- (iii) Tchi2 analcime sandstones, composed of a detrital fraction (quartz, K feldspars, albite, muscovite) and secondary assemblage (diagenetic and postdiagenetic alteration) related to the presence of analcime, chlorite, illite and other clay minerals. The analcime of these facies occurs as automorphous crystals in the pores.
- (iv) The Tchi2 analcimolites, similar to the Abinky quartz-analcimolite facies but with a greater presence of detrital fraction due to its location in Tchi2.

Each of the samples was subjected to the following treatment: the samples were cut off from their preserved undried core with a diamond saw cooled under a constant water flow and were left to air-dry for 1.5 days. Afterward, each sample was placed in a plastic bag and crushed with a hammer before being ground for 6 minutes in a Retsch RM 200 electric agate mill. Milli-Q® (18.2 MΩ.cm) water was then added to these rock powders to obtain suspensions with a solid/liquid ratio of approximately 4 g per 10 mL. Finally, the rock/water mix was ground a second time using a micronizing mill (XRD–Mill McCrone) for 7 minutes to obtain a micron-scale (< 5 µm) total powder. Note that this particle size was chosen to obtain reliable crystallite statistics in XRD analysis (Klug and Alexander, 1954). The suspensions were dried in a ventilated oven at 60 °C; dried solids were redispersed in Milli-Q® water to perform three 8-hour cycles of dialysis to remove any traces of salts. Finally, dialyzed suspensions were placed at 60 °C in a ventilated oven and, once dried, sieved to 50 µm to disperse the aggregates. These dispersed powders will be referred to as "total rock powders" and were used for XRD pattern acquisition and cationic exchange experiments.

2.2. **Solid characterization**

2.2.1. X-ray powder diffraction and Rietveld refinement setup

X-ray powder diffraction was conducted on a Bruker D8 Advance equipped with a LynxEye detector. Patterns were acquired in a Bragg–Brentano geometry using CuK$\alpha_{1,2}$ ($\lambda_{\overline{K\alpha 1,2}}$ = 1.5418 Å) in the 2-65 °2θ angular range, with an angular step of 0.02°2θ and a counting time of 0.6 s per step. The analytical conditions were set to 40 kV/40 mA. Rietveld (Rietveld, 1969) refinements were carried out using BGMN software (Bergmann and Kleeberg, 1998) associated with the PROFEX interface (Doebelin and Kleeberg, 2015). Rietveld quantification of both crystalline and amorphous phases was performed via the

addition of ZnO (Zincite: Sigma–Aldrich, RaegentPlus® powder, < 5 µm, 99.9%) as an internal standard in each sample powder. To obtain homogeneous powders, the internal standard was manually combined with the sample in an agate mortar, and the overall powder was sieved to 50 µm to disperse potential aggregates. XRD patterns were systematically collected with 0.5 ± 0.05 g of these mixed powders. As a first step toward natural sample quantification, synthetic mixtures containing three crystalline phases (quartz, analcime and ZnO) were prepared to assess the effect of the amount of internal standard (10 *vs.* 30wt%) on the quantification results.

Table 1: Weighted proportions of the three crystalline phases in the synthetic mixtures as a function of internal standard quantity.

	10wt% Zincite				30wt% Zincite			
	Mix 1a	**Mix 1b**	**Mix 1c**	**Mix 1d**	**Mix 2a**	**Mix 2b**	**Mix 2c**	**Mix 3c**
%Analcime	0.0	24.8	50.0	74.3	0.0	19.3	38.8	58.1
%Quartz	89.9	65.2	40.1	15.2	70.0	50.6	31.1	11.9
%Zincite	10.1	10.0	9.9	10.5	30.0	30.1	30.0	30.0

Thus, eight synthetic samples (Table 1), characterized by different weighted proportions of quartz (from Poitiers University collection), cubic analcime natural crystals (from Rio Grande Do Sul, Brazil) and zincite powder, were prepared and analyzed following the aforementioned protocols (Section 2.2.1.).

2.2.1.1. Rietveld refinement of natural samples

The structures and chemical compositions of each identified mineral phase (Fig. S3.i) used for quantification were taken from the Profex database for anatase (04-007-0701), hematite (04-003-2900), goethite (04-015-2898), quartz (04-008-4821), zincite (04-003-

2106), and disordered chlorite/biotite (Bergmann and Kleeberg, 1998) and from the literature for albite (Harlow, 1982), microcline (Bailey, 1969), calcite (Markgraf and Reeder, 1985) and tetragonal analcime (Mazzi and Galli, 1978). An analog structure model was chosen for natural samples based on petrographic observations showing a nontotal extinction under cross-polarized light as well as on the presence of the (200) and (210) reflections in the experimental XRD patterns (Fig. S3.). The same crystal structure was used for the Rietveld refinement of analcime belonging to synthetic mixtures, and the only difference was that the lattice parameters were tuned to agree here with a true cubic crystal system (a=b=c), as indicated by the lack of 210 and 200 reflections for this mineral (Fig. S3). In addition, to reach the optimal refinement of analcime minerals and enforce a neutral structural formula, the chemistry of the phase was allowed to vary in agreement with the results and boundary sets obtained by EDS measurements (see next Section 2.2.1.2.). Accordingly, the Rietveld refinement optimized the chemistry of the analcime of each natural sample based on the structural formula $Na_y(Fe_{(3-x)}[AlSi]_x)O_6 \cdot nH_2O$ with the following constraints: $1.95 < x < 3$ (1.95 being the minimum Si measured by EDS, see Fig. 4), $0 < y < 1$, $0 < n < 1$ and $(x + y) \geq 3$. $Fe_{(III)}$ was used since this element was detected by EDS and can be classically found in analcime tetrahedral sites (Calleri and Ferraris, 1964; Ratterman and Surdam, 1981; Luhr and Kyser, 1989; Wilkinson and Hensel, 1994; Deer et al., 2004; Azizi and Yousefpour, 2011). Note that due to poor electronic contrast between silicon and aluminum, only- silicon atoms are considered in the refinement. However, aluminum remains amalgamated in the refined quantity of silicon $(x = Al + Si)$. Aluminum and silicon are later decorrelated via $Al = (y - x) - 3$ and $Si = x - Al$. Finally, the quality of the Rietveld refinements was assessed with χ^2 parameters (Toby, 2006).

2.2.1.2. SEM/EDS analyses and total rock chemistry

Chemical analyses were performed to quantify major element concentrations in the 37 rock samples. These values were obtained by using a method based on total lithium borate fusion prior to acid dissolution and ICP–AES analyses.

Local chemical microanalyses using Energy Dispersive Spectroscope (EDS) coupled with Scanning Electron Microscope (SEM) (JEOL JSM5600 LV) were performed on carbon-coated, polished, thin sections for 16 of the 37 samples considered representative of the 4 facies studied (presented in Section 2.1.). Analyses were performed using the backscattered electron mode, with an acceleration voltage of 15 kV and a probe current of 1 nA. The same conditions were used for standard analyses (albite (Si, Al, Na), diopside (Ca), almandine (Mg, Fe), orthose (K), spessartine (Mn), gypsum (S) and Ti metal (Ti)). Problems associated with measurements of Na by X-ray spectrometry (EDS or WDS) have been reported in the literature, including for the zeolite family (Campbell et al., 2016) which is especially true for analcime (Deer et al., 2004). For this latter, authors have found that the count rates of sodium decreases over time when the electron beam is focused on a single point. Then, as recommended by these previous authors, the analyses were carried out with a defocused beam and acquired over short counting times (5 seconds) to minimize the loss of sodium under the beam.

2.2.2. Ion-exchange experiments and modeling

2.2.2.1. Experiments

Ion-exchange experiments were performed on the total rock powder samples (*i.e.*, the same samples as those characterized with the Rietveld refinement method). Two types of ion-exchange experiments were carried out. The first one was performed to assess the maximum

295 amount of exchangeable Na in the 37 samples (acetate ammonium method; referred to
296 CEC_{Na/NH_4}). For that, the NH_4^+ probe was chosen due to its high selectivity toward Na^+
297 cations in the analcime structure (Barrer and Hinds, 1953; Barrer, 1981; Pesonen et al., 2021).
298 The second was Na^+/H^+ exchange performed at different pH values for 4 samples of the
299 Abinky analcimolite facies (labeled W009b, X031a, X032a and X035) and characterized by
300 the presence of only analcime and chlorite with analcime contents higher than 67wt%.

301 Na^+/NH_4^+ experiments were carried out with 1 M ammonium acetate at neutral pH (7.1 ±
302 0.3) with a solid/liquid ratio of 30 ± 0.6 g/L for 48 hours. To correct for the effect of the
303 potential dissolution of Na phases (analcime and albite) present in the samples, control
304 batches were established with Milli-Q® water using the same solid/solution ratio and duration
305 and at around the same pH than those measured for the Na^+/NH_4^+ experiments. This pH value
306 was chosen based on preliminary kinetic results showing that 48 hours of exchange was
307 sufficient to obtain a constant amount of exchanged Na.

308 Na^+/H^+ exchange experiments were carried out in two ways: (i) with HCl using a solution
309 of 3.3×10^{-3} M HCl (pH 2.5) and (ii) with H_2SO_4 using a solution of 3.3×10^{-3} M H_2SO_4 (pH
310 2.5). In both experiments, different solid/solution ratio values were tested ranging from 10 to
311 100 g/L. This method allows us to vary the final pH from ~3.5 to 6.5. In these experiments,
312 total rock dissolution was determined by measurements of (i) aqueous silica concentration
313 obtained using the molybdate blue method (Strickland and Parsons, 1972) *via*
314 spectrophotometry at 820 nm and (ii) aqueous aluminum concentration obtained by the
315 eriocrome cyanine R. colorimetry method via spectrophotometry at 585 nm; the latter method
316 was adapted from Shull and Guthan (1967) from the initial procedure of Knight (1960). To
317 assess the dissolution of analcime from that of chlorite, aqueous Mg measurements were
318 carried out by Atomic Absorption Spectrometer (Varian® AA240FS) (AAS). The assay

319 solutions were prepared in 2% HNO_3 with 5 g/L $SrCl_2$ to consider potential interferences
320 during the analysis of Mg^{2+} concentrations. To assess the dissolution of the solid, the samples
321 before and after acidification were characterized by XRD (see Section 2.2.1.) and by infrared
322 spectrometry using a Thermo Scientific (Nicolet 6700®) Integrating Sphere Near-IR in
323 diffuse reflectance mode and InGaAs detector. A white light source and a CaF_2 separator were
324 used for a spectral range from 12000 cm^{-1} to 3800 cm^{-1} at a step size of 4 cm^{-1}.

325 For the two ion-exchange experiments (Na^+/NH_4^+ and Na^+/H^+) and the control
326 experiments performed in Milli-Q®, which were carried out for 48 hours, the suspension was
327 stirred at room temperature. Each suspension was finally centrifuged at 4000 rpm for 10 min
328 to separate the supernatant from the solid slurry. For analyses of the aqueous phase, the
329 supernatant was filtered using a 0.45 µm syringe cellulose filter, and aqueous Na was
330 determined by AAS. The assay solutions were prepared in 2% HNO_3 with 2 g/L KCl to
331 consider potential interferences during the analysis of Na^+ concentrations. For all batches, the
332 final pH value was measured immediately after the experiment using a combined pH
333 electrode calibrated using 4 pH buffer solutions (pH 1.68, 4, 7 and 10). Because the electrode
334 was stored in KCl solution, these measurements were performed on separate aliquots to avoid
335 any contamination of the aqueous samples. The amount of adsorbed Na was obtained from the
336 maximum amount of Na adsorbed ($CEC_{max_{Na/NH_4}}$) and the final Na aqueous concentration
337 ($Na_{des_{Na/H}}$) according to:

338 $$Na_{ads} = CEC_{max_{Na/NH_4}} - Na_{des_{Na/H}} \quad (1)$$

339 For the Na^+/NH_4^+ and Na^+/H^+ exchange and Mg measurement, a classical error calculation
340 was used to associate each measured value with a minimum error value (ΔC) calculated
341 according to the error propagation law (Barrante, 1974):

$$\Delta C = \sqrt{\left(\frac{C_c \cdot V}{m}\right)^2 \times Q^2} \quad (2)$$

where C_c is the concentration obtained by AAS for Na and Mg and by colorimetry for Al and Si, V is the volume of exchange solution (NH_4^+, HCl or H_2SO_4), and m_d (g) is the mass of dry solid after dehydration at 65 °C. Q^2 is a constant equal to 0.38 for AAS and 0.08 for colorimetry, obtained using preliminary tests acquired on triplicates of the same samples.

2.2.2.2. Ion-exchange modeling

Experimental data relative to the Na^+/H^+ experiments were interpreted using an exchange model. Calculations were performed using Phreeqc® software (Parkhurst and Appelo, 1999) associated with the Thermoddem database (Blanc et al., 2012). Modeling was based on a single-site called >Xa site for which the total amount is fixed to the CEC_{Na/NH_4} value specific to each sample (the maximum amount of Na that analcime can exchange under our experimental conditions) and measured as explained in the previous section. As the Na^+/H^+ exchange experiment was performed for solid/solution ratios ranging from 10 to 100 g/L, the amount of input site was related to the amount of solid used for each batch, *i.e.*:

$$> Xa = CEC_{Na/NH_4} \times \text{SL ratio} \quad (3)$$

where CEC_{Na/NH_4} is in eq/L and SL ratio is the solid/solution ratio in g/L to express >Xa in eq/L.

Finally, as the 4 samples for which experimental data were acquired presented the same mineralogical characteristics (*i.e.*, differing only in their proportion of analcime content; see Section 2.2.2.1.), the four datasets were reproduced by using the same Na^+/H^+ exchange selectivity coefficient ($\log K_{Na/H}$) associated with the chemical reaction $> NaXa + H^+ \rightarrow > HXa + Na^+$, and this selectivity coefficient is defined according to:

$$\log K_{Na/H} = \frac{E_{H^+} \times [Na^+]_{aq} \times \gamma_{Na^+}}{E_{Na^+} \times [H^+]_{aq} \times \gamma_{H^+}} \quad (4)$$

where E_{H^+} and E_{Na^+} are the equivalent fractions of H^+ and Na^+ sorbed on the solid, respectively, γ_{H^+} and γ_{Na^+} are the activity coefficients for the H^+ and Na^+ aqueous species calculated with the Davies approximation and $[H^+]_{aq}$ and $[Na^+]_{aq}$ are measured aqueous concentrations.

3. Results and discussion

3.1. Rock mineralogy and analcime crystal chemistry

Mineralogical quantification based on Rietveld refinement allows the quantification of both crystalline and amorphous phases ($wt\%_{Riet.}$) present in rocks via the use of an internal standard. By refining the average structural formula and the quantity of each crystalline mineral phase, this method allows recalculation of the amount of oxides ($ox\%_{Riet.}$) present in each sample and, consequently, their total chemistry. Total rock chemistry was also measured independently on each sample (ICP–AES, see 2.2.1.2.), challenging the Rietveld calculation to validate the method.

3.1.1. *Validation of phase quantification using synthetic samples*

Fig. 1 shows a comparison of experimental results ($wt\%_{exp.}$; based on measured weight) and Rietveld refinement ($wt\%_{Riet.}$) for synthetic mixtures differing in the amounts of quartz, analcime and zincite (Table 1). For each of the eight mixtures, no amorphous phases were quantified by Rietveld refinement irrespective of the content of internal standard used (*i.e.*, 10wt% and 30wt%). This allows us to state that such a quantification method also correctly reflects noncrystalized material proportions in the samples even in an amorphous-free case. With the moderately complex mixture studied here and appropriate preparation (see Section

2.2.1.), there is an average difference between $wt\%_{exp.}$ and $wt\%_{Riet.}$ less than ± 2wt% (Madsen et al., 2019). Finally, an increase in the internal standard from 10 to 30wt% did not deteriorate the crystalline phase quantification. According to these results, one can reasonably assume that the Rietveld quantification method used is valid. Consequently, 30wt% ZnO was chosen as the natural sample internal standard proportion. Such a quantity appears to be the best compromise to correctly quantify the proportion of amorphous phases in the XRD patterns irrespective of their amount in the rock samples (Jones et al., 2000; Westphal et al., 2009) while maintaining a satisfactory quantification of the crystallized phases.

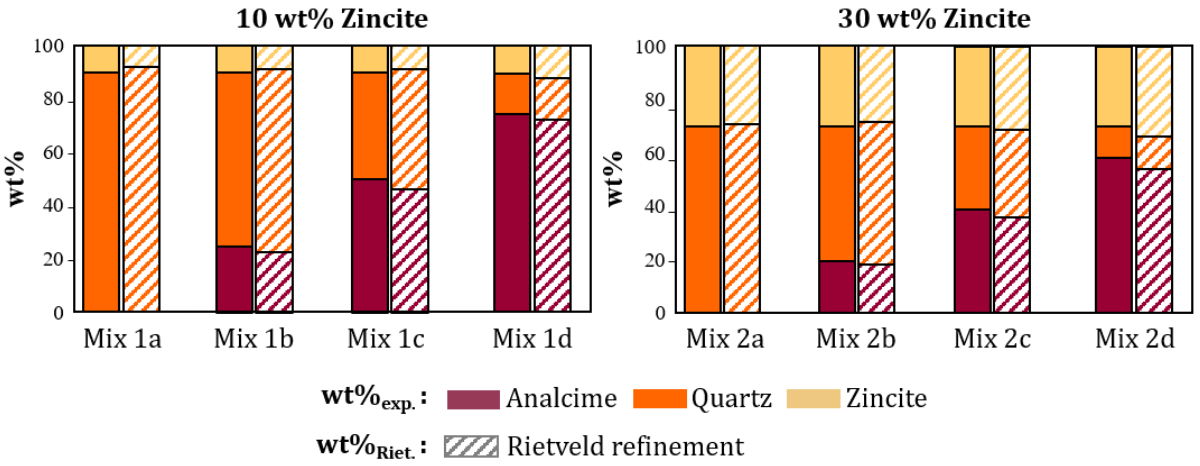

Figure 1: Comparison of the weighed experimental data ($wt\%_{exp.}$) and the Rietveld refinement data ($wt\%_{Riet.}$) for synthetic three-phase mixtures composed of quartz, analcime and zincite crystals in varying proportions, using two weight percentages for the internal standard (zincite).

3.1.2. Comparison between mineralogical and chemical rock data

Based on the previously validated Rietveld refinement protocol, amorphous and crystalline phases were quantified. The chemical formulas of the latter were expressed as

oxide percentage weighted by their proportion, allowing for a total sample chemistry recalculation. Such results ($ox\%_{Riet.}$) is directly comparable with the total experimental oxide proportion ($ox\%_{exp.}$) obtained by total rock chemistry.

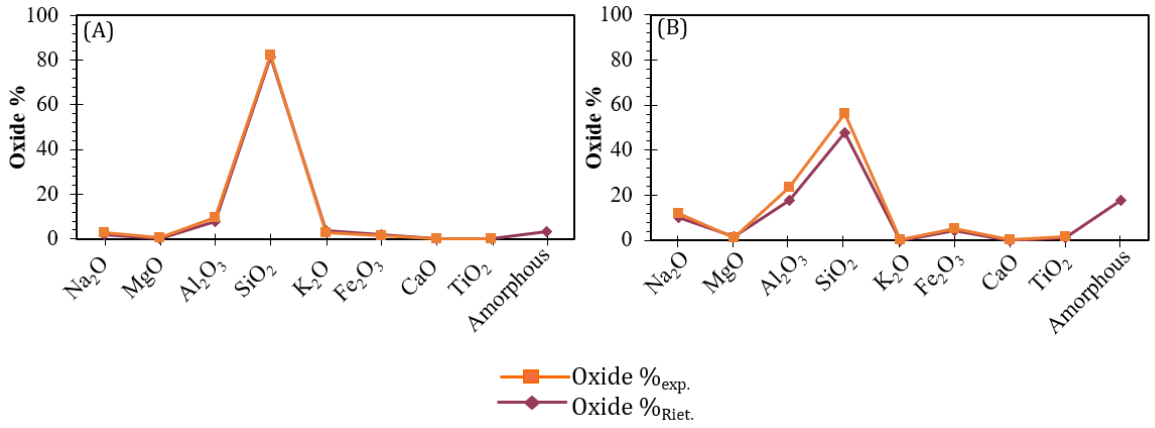

Figure 2: Comparison of the total oxide percentages ($ox\%_{exp.}$) obtained using rock total chemistry data with those calculated from Rietveld refinement ($ox\%_{Riet.}$). Data are plotted for two natural samples: (A) a sample from the Tchi2 analcime-sandstone facies with a low content of amorphous phases (~3wt%$_{Riet.}$) and (B) a sample from the Abinky analcimolite facies having a high content of amorphous phases (18wt%$_{Riet.}$).

The results are presented in Fig. 2, in which data are plotted for two samples differing in their contrasting amounts of amorphous phases (2A: ~3wt%$_{Riet.}$ *vs.* 2B: ~18wt%$_{Riet.}$). In the case of the sample containing only ~3wt%$_{Riet.}$ of amorphous phases (Fig. 2A), good agreement is observed between $ox\%_{exp.}$ and $ox\%_{Riet.}$ with a mean absolute error of 1%. Additionally, in the case of the sample containing ~18wt%$_{Riet.}$ of amorphous phases, good agreement is observed between $ox\%_{exp.}$ and $ox\%_{Riet.}$ for most of the oxides studied, *i.e.*, Na_2O, MgO, K_2O, Fe_2O_3, CaO and TiO_2, also with a mean absolute error smaller than 1%, which is the case for all the samples. The highest difference is found for Al_2O_3 and SiO_2 (5.9 and 8.8wt%,

respectively) and is due to the presence of amorphous phases for which the chemistry cannot be accounted for in $ox\%_{Riet.}$ (*i.e.*, only the chemistry of the crystalline phases is included in the total chemistry refined by the Rietveld method). In addition, because the $ox\%_{exp.}$ for SiO_2 and Al_2O_3 are consistently higher than the $ox\%_{Riet.}$ values, we can reasonably assume that the amorphous phases responsible for the discrepancy are mainly composed of Si and Al

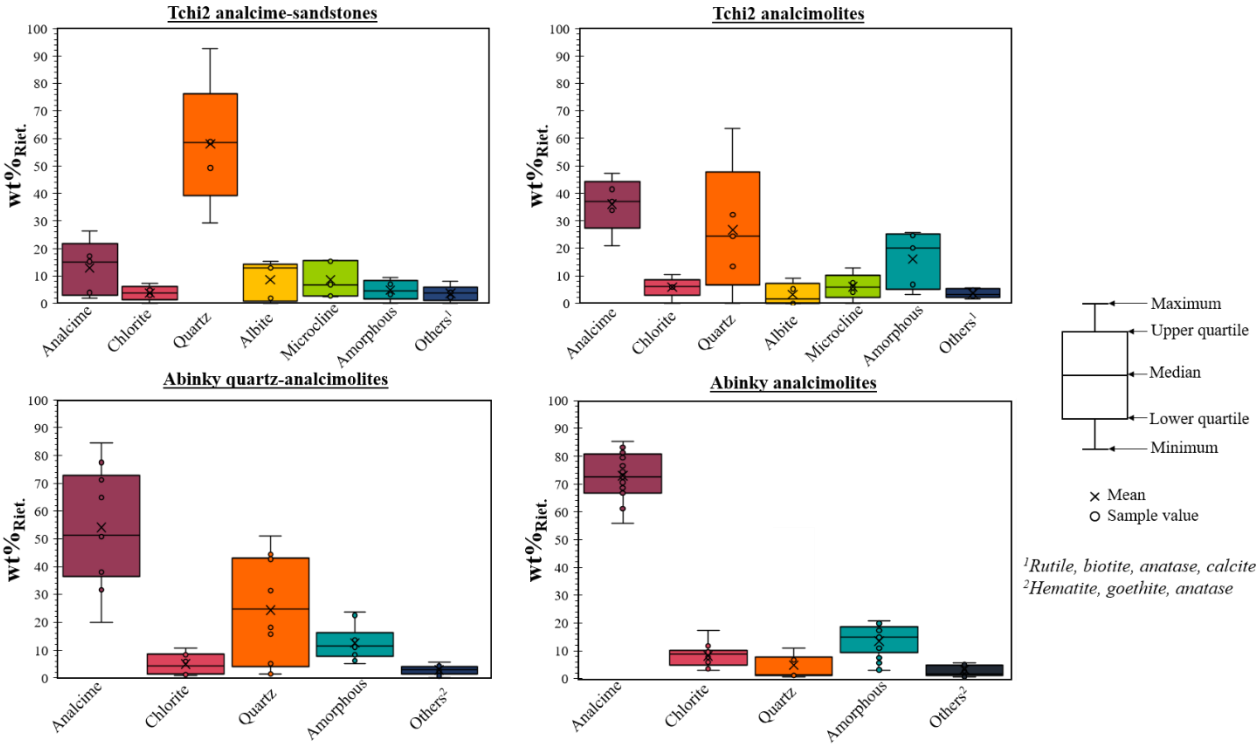

elements. Finally, for the 35 other samples, a significant amount of amorphous phases is systematically detected using the Rietveld method in samples with a difference between Si and Al ox% deviating by more than 1%. These cross-technique results allow us to fully validate the mineral quantification procedure.

Figure 3: Proportions ($wt\%_{Riet.}$) of crystalline and amorphous phases obtained by Rietveld refinement for the four facies of interest (see Section 2.1). As detailed in the text, the method used to obtain these data involved the use of 30wt% ZnO as the internal standard in the

437 samples. This entire quantified dataset has an average χ^2 value of 2.67 with a standard
438 deviation of 0.63.
439
440 The Abinky analcimolites facies (Fig. 3) have the highest analcime content
441 (*i.e.*, > 56wt%$_{Riet.}$), followed by the Abinky quartz-analcimolite facies (*i.e.*, > 20wt%$_{Riet}$).
442 Literature studies report a similar tendency for samples from formations composed mainly of
443 analcime (Pacquet, 1968; Valsardieu, 1971; Billon, 2014; Billon and Patrier, 2019). The
444 Tchi2 analcimolite facies also shows a high analcime content (*i.e.*, > 21wt% $_{Riet.}$) even though
445 the latter is located within the Tchi2 formation, defined in the literature as an arkosic
446 sandstone formation (Billon, 2014; Billon and Patrier, 2019), explaining the higher proportion
447 of quartz and other detrital minerals inherent to the Tchi2 formation.
448
449 *3.1.3. Discussion on analcime crystal chemistry*
450 Data relative to analcime chemistry (*i.e.*, contents of Al and Si) obtained by Rietveld
451 refinement and EDS/SEM local analysis were compared to the chemistry of natural analcimes
452 found in various environments (Coombs, 1955; Yoder Jr and Weir, 1960;Wilkinson and
453 Whetten, 1964; Harada et al., 1967; Seki and Oki, 1969; Harada and Nagashima, 1972;
454 Sheppard and Gude, 1973; Walton, 1975; Mazzi and Galli, 1978; Ratterman and Surdam,
455 1981; Johnson et al., 1982; Bargar and Beeson, 1985; Broxton et al., 1987; Wise and Kleck,
456 1988; Luhr and Kyser, 1989; Karlsson and Clayton, 1991; Wilkinson and Hensel, 1994; Tang
457 et al., 1997; Wilkin and Barnes, 1998) and are reported in Fig. 4. $Fe_{(III)}$ was not considered in
458 this comparison, as this element only represents, at maximum, 3% of the isomorphic
459 substitutions in the analcime structure (*i.e.*, 97% were due to $Al_{(III)}$ for $Si_{(IV)}$ substitutions).
460 The results obtained in this study, whether by SEM/EDS or the Rietveld procedure, show the

same range of Si and Al contents as those reported in the literature, in which the Si/Al ratios are bounded by 1.5 and 3.1 (Wilkinson and Whetten, 1964; Ratterman and Surdam, 1981). In the literature dataset and in this study, there is no correlation between the geological origin of the analcime and the amount of tetrahedral substitution. The variability in the crystal chemistry of the studied samples covers the entire range of Si/Al ratios that analcime can contain. Nevertheless, in Fig. 4, the chemical analysis density repartitioning tends to point toward the analcime formula: $Na_{0.94}Al_{0.94}Si_{2.06}O_6.H_2O$.

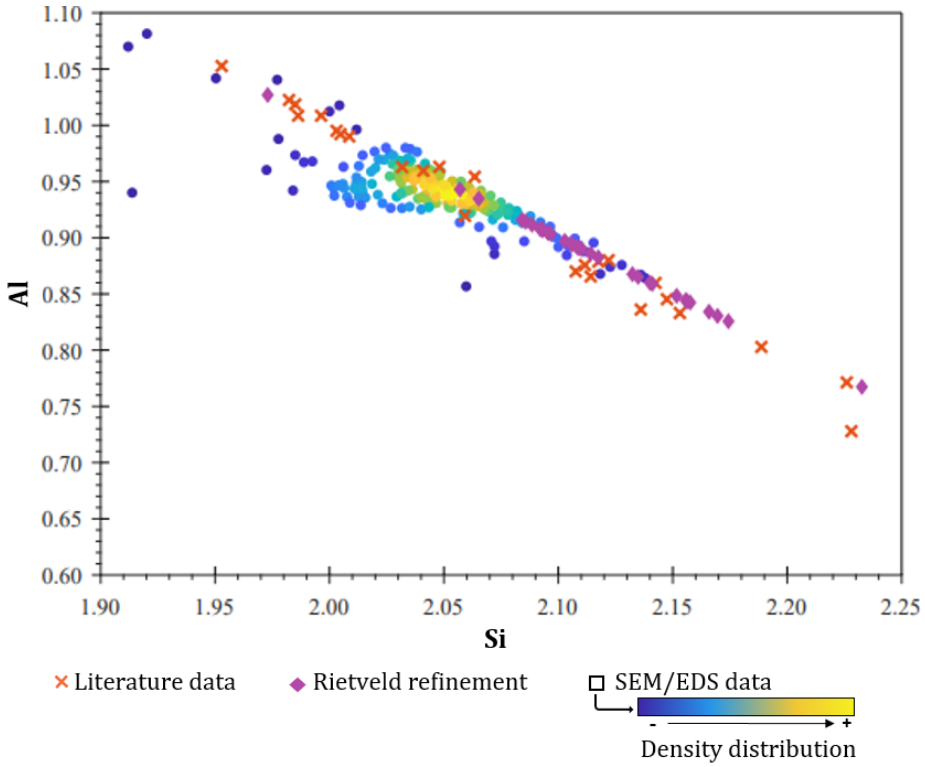

Figure 4: Comparison of analcime chemistry between data from the literature (Coombs, 1955; Yoder Jr and Weir, 1960;Wilkinson and Whetten, 1964; Harada et al., 1967; Seki and Oki, 1969; Harada and Nagashima, 1972; Sheppard and Gude, 1973; Walton, 1975; Mazzi and Galli, 1978; Ratterman and Surdam, 1981; Johnson et al., 1982; Bargar and Beeson, 1985; Broxton et al., 1987; Wise and Kleck, 1988; Luhr and Kyser, 1989; Karlsson and Clayton, 1991; Wilkinson and Hensel, 1994; Tang et al., 1997; Wilkin and Barnes, 1998) obtained for

475 analcimes located in different geological formations and data obtained in this study by
476 Rietveld refinement and SEM/EDS local analysis. For the latter, a 2D density plot, with a
477 mean value of Si=2.05 and Al=0.94, was reported to better appreciate the dispersion of the
478 dataset .
479
480 A detailed plot of the values acquired by SEM/EDS is presented in Fig. S5. One should
481 note that a slight increase in structural charge is observed for the Abinky analcimes, followed
482 by the Tchi2 analcime sandstones. Further investigation should be performed to understand
483 this observation.
484
485 **3.2. Ion exchange**
486 *3.2.1. Experimental Na^+/NH_4^+ exchange at neutral pH*
487 Fig. 5 shows the $wt\%_{Riet.}$ of analcime as a function of the Na exchanged by the NH_4^+ ion
488 (Na^+/NH_4^+ batches). Exchange experiments were performed for the 37 samples of the four
489 facies of interest, and for each sample, a correction for dissolution was made. The average pH
490 value of the Na^+/NH_4^+ exchange was approximately pH 7.1 ± 0.2, which allowed us to
491 compare the amounts of exchanged Na^+ in all 37 samples studied.

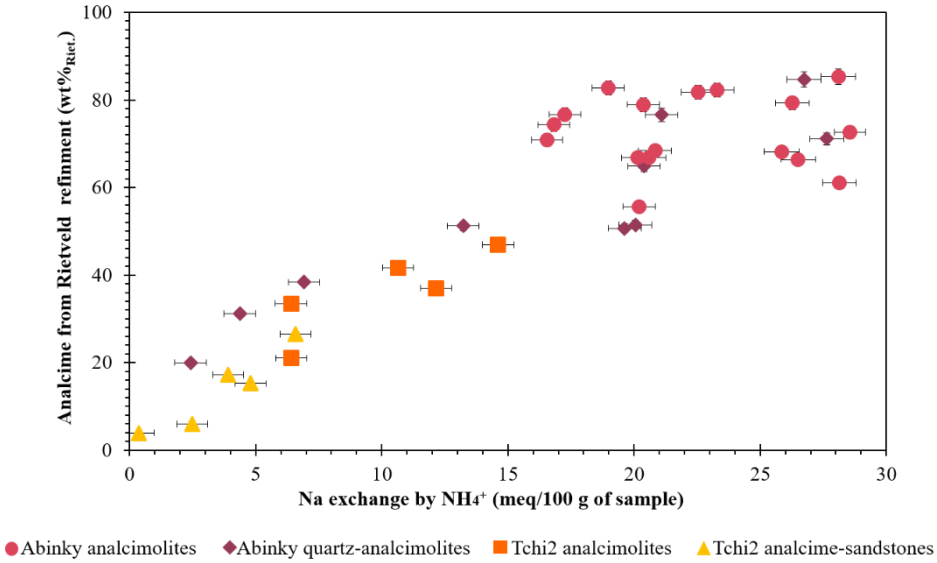

492 Figure 5: Evolution of the analcime percentage (wt%$_{Riet.}$) obtained by Rietveld refinement as a
493 function of the amount of Na^+ exchanged with 1 M NH_4^+. Experiments were carried out for
494 the four facies of interest under the same experimental conditions (same particle size fraction,
495 48 h of exchange at 25 °C and solid/solution ratio of 30 g/L). The data were corrected for the
496 potential dissolution of analcimes by using data obtained from Milli-Q water control
497 experiments (see text for details of this correction).

498

499 The amount of Na^+ exchanged is directly correlated with the analcime content obtained by
500 the Rietveld method. The more analcime a sample contains, the more Na^+ is exchanged. Thus,
501 the samples with the lowest analcime content, *i.e.*, the Tchi2 analcime sandstones from 4 to
502 27wt%$_{Riet.}$ (see Fig. 3), exchange between 0.4 and 6.6 meq/100 g of Na^+. The most analcime-
503 rich facies, *i.e.*, the Abinky analcimolites, which have analcime contents from 56 to 85wt%$_{Riet.}$
504 (see Fig. 3), exchanges between 17 and 29 meq/100 g of Na^+. As discussed in Section 3.1.3
505 and presented in Fig. S5, there is variability in the crystal chemistry of analcimes. However,
506 despite this variation and because the correlation is close to linearity between the amount of
507 Na^+ exchanged by NH_4^+ and analcime content, we can reasonably assume in a first

approximation that the selectivity coefficient describing Na^+/NH_4^+ exchange is independent of the structural charge of the analcime present in the samples used.

For each sample, the total stock of Na^+ (Na_{tot}) was calculated from a single cationic formula. This single formula derives from the mean value of the 2D density plot of the SEM-EDS analyses (Fig. 4).

$$Na_{tot} = \frac{wt\%_{MEB/EDS}}{\left(\sum atom_i \times M_{atom_i}\right)} \quad (5)$$

where Na_{tot} is expressed in meq/100 g, and "$atom_i$" is the number of 'i' atoms in the structural formula obtained by MEB/EDS (with "i' equal to Si, Al, $Fe_{(III)}$, Na, and O atoms and H_2O molecules). Calculations were made by using the structural formula issued from the mean value of the 2D density plot (*i.e.*, $Na_{0.87}(Fe_{0.03}Al_{0.94}Si_{2.05})O_6.nH_2O$). M_{atom_i} is the molar mass (g/mol) of the atom i.

The Na_{tot} values were then compared to the CEC_{Na/NH_4} values to obtain the proportion of Na^+ exchanged by NH_4^+. Na_{tot} is very high in the analcime: 454.3 meq/100 g for a pure theoretical analcime crystal phase with the composition $NaAlSi_2O_6.H_2O$. Furthermore, an average value of ~6.2±1.4% of Na is exchanged among the 37 samples with these experimental conditions using a 1 M NH_4^+ solution. Then, even with this small proportion, a maximum CEC_{Na/NH_4} equal to 30 meq/100 g can be obtained for the sample characterized by the highest analcime amount ($85wt\%_{Riet.}$).

3.2.2. Na^+/H^+ exchange: experiment and modeling

3.2.2.1. Exchange *vs.* dissolution contributions

Total aqueous Mg ($Mg_{aq_{tot}}$) was measured in the supernatants of the batches $(Na^+/H^+)_{Cl}$ of the four Abinky analcimolite samples (W009b, X031a, X032a and X035; see Section

2.2.2.1.). In these samples chlorite is the only Mg-bearing phase and represents ~10wt%$_{Riet.}$ (see Fig. 3). Thus, from $Mg_{aq_{tot}}$, it is possible to calculate the percentage of dissolution of chlorite considering a cationic formula approximated by the MEB/EDS analysis of $(Si_{2.83}Al_{1.17})O_{10}(Fe_{3.33}Al_{1.25}Mg_{1.08}Ti_{0.1}Mn_{0.02})(OH)_8$. Thus, for pH varying from ~ 3.5 to 6.5 and considering stoichiometric dissolution, the amount of chlorite dissolution is only from 1.2 to 0.1wt%. From $Mg_{aq_{tot}}$, it is possible to obtain the contribution of Si_{aq} originating from the dissolution of chlorite ($Si_{aq_{chl}}$) and thus obtain the Si_{aq} from the dissolution of analcime ($Si_{aq_{Ana}}$), considering stoichiometric dissolution and based on $Si_{aq_{ana}} = Si_{aq_{tot}} - Si_{aq_{chl}}$. Due to the low chlorite content in the samples and because chlorite only dissolves to a limited extent, chlorite dissolution only accounts for an average of approximately 0.1% of the $Si_{aq_{tot}}$ measured in the supernatants. Thus, the large majority of $Si_{aq_{tot}}$measured in the supernatants comes from the dissolution of analcime. Dissolution of chlorite is then considered negligible under the acidic conditions used in this study (*i.e.*, pH > 3.5).

The aqueous $Na_{des}/Si_{aq_{tot}}$ ratios (written Na/Si hereafter) obtained from these measurements are presented in Fig. 6. In the case in which the only reaction consuming H^+ in the experiments was the dissolution of analcime, and considering a theoretical formula of $NaAlSi_2O_6.H_2O$ and that this dissolution was stoichiometric, the aqueous Na/Si measured in the supernatant should be ~ 0.5. The exact ratio obtained from the MEB/EDS measurements is represented by the black line in Fig. 6 and corresponds to an average calculated value from

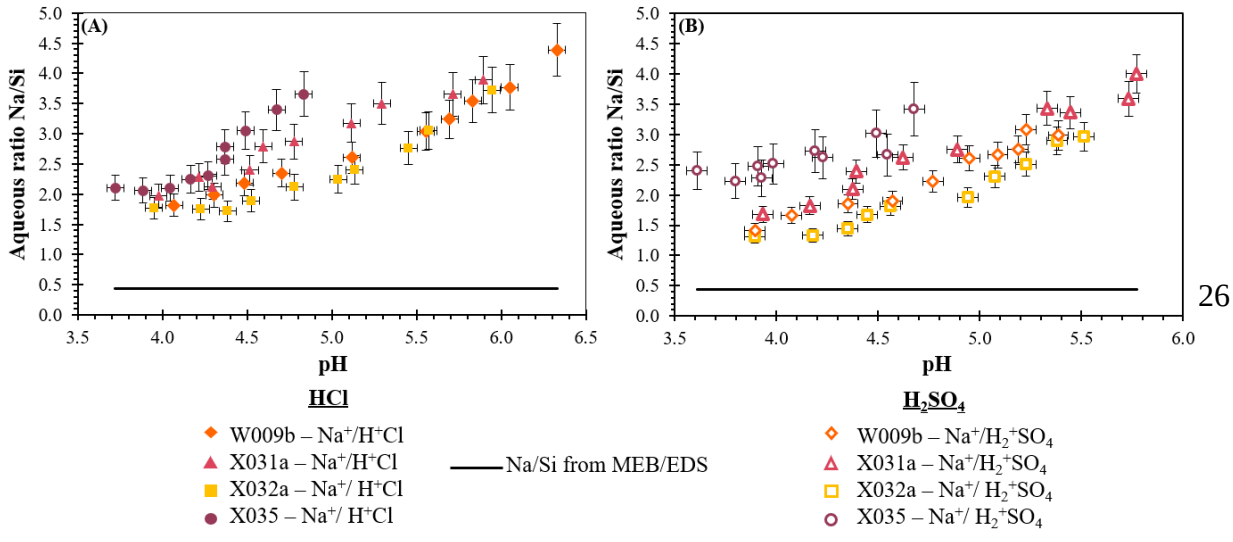

550 0.427 to 0.449 in the samples. The overall Na/Si measured for the four samples used in the pH
551 range probed (between 3.1 and 6.3) was consistently greater than 1.3 for experiments
552 performed in both chloride and sulfate media (*i.e.*, $(Na^+/H^+)_{Cl}$ and $(Na^+/H^+)_{SO_4}$). Thus, this
553 high ratio measured in the supernatant could be explained by cation exchange between the
554 sodium that is naturally present in the analcime structure, allowing us to counterbalance its
555 negative charge, and aqueous protons in solution.
556 Figure 6: Comparison of the aqueous Na/Si ratio measured in supernatants after Na^+/H^+
557 exchange and Na/Si ratio of analcime obtained by MEB/EDS analysis. Data are reported as a
558 function of pH and for 4 Abinky analcimolites (see Section 2.2.2.2. for details). (A) Data
559 obtained in chloride medium. (B) Data obtained in sulfate medium. For both media,
560 experimental data are represented as symbols, and the Na/Si ratio of the analcime obtained by
561 MEB/EDS is represented by a straight line.
562
563 The total $Al_{aq_{tot}}$ was measured in the supernatants for the lowest pH (*i.e.*, corresponding
564 to conditions for which $Si_{aq_{tot}}$ is most significant) of each sample for $(Na^+/H^+)_{Cl}$. As the
565 dissolution of chlorite was negligible as mentioned above, Al_{tot} measured in the supernatant
566 could be only attributed to analcime dissolution. Thus, Na_{des}/Al_{tot} were calculated and equal to
567 3.03, 4.18, 4.80 and 2.17 for W009b, X031a, X032a and X035, respectively. Because the
568 stoichiometric dissolution of analcime should lead to a ratio close to 1 (see structural
569 formula), these data, like the Si_{aq} experimental data, suggest that a significant proportion of
570 H^+ is consumed through Na^+ exchange.
571 Thus, for the whole pH range studied, based on $Si_{aq_{tot}}$ data measured throughout the
572 $(Na^+/H^+)_{Cl}$ and $(Na^+/H^+)_{SO_4}$experiments and considering the stoichiometric dissolution of
573 analcime, the maximum percentage of analcime that can be dissolved during the experiments

574 is 0.3 wt%. Moreover, for the aqueous concentrations measured for pH, Na, Al and Si,
575 thermodynamic calculations showed that all supernatants were oversaturated with respect to
576 amorphous silica phases. Note that XRD and infrared spectroscopic measurements confirmed
577 the absence of newly formed phases in our samples, even at the lowest pH tested (*i.e.*, pH
578 approximately 3.7). Moreover, note that a Rietveld refinement with an internal standard was
579 carried out on the samples after acidification. Results showed no significant variation of
580 mineralogy between non-acidified and acidified samples as well as no change in the amount
581 of amorphous phase after acidification. Thus, with this information, the CEC will be
582 considered as consistent during the procedure used afterward to assess a selectivity coefficient
583 value describing Na^+/H^+ exchange within the pH range studied for the four samples used and
584 for both chloride and sulfate media.
585
586 3.2.2.2. Thermodynamic modeling of Na^+/H^+ exchange
587 Fig. 7 compares the amount of adsorbed Na^+ (*i.e.*, Na_{ads}; see Eq. 1.) measured
588 experimentally as a function of pH for the 4 samples studied with (i) the nature of the counter
589 ion (*i.e.*, Cl^- or SO_4^{2-}) and (ii) the CEC_{Na/NH_4}values measured for each of these samples at
590 neutral pH (~7.35). Because the shape of the experimental Na^+/H^+ isotherms was consistent
591 with ion exchange at a single site and because Na_{ads} measured at the highest pH value
592 investigated during the Na^+/H^+ isotherm (~pH 6.5) approaches the CEC_{Na/NH_4} measured at
593 neutral pH, modeling was performed by considering a unique site for which the sorption site
594 density is equal to CEC_{Na/NH_4}. This assumption, already mentioned in Section 2.2.2.2, is
595 equivalent to considering that NH_4^+ and H^+ ions can probe the same amount of Na^+ in the
596 analcime structure. First, the same log $K_{Na/H}$ value was used to interpret the whole dataset
597 acquired for the four samples for the $(Na^+/H^+)_{Cl}$ isotherms (black points). A rather good

agreement between the experimental data and predicted data can be observed (see Fig. 7), and the average log $K_{Na/H}$ value that allowed us to interpret this whole dataset is 1.3.

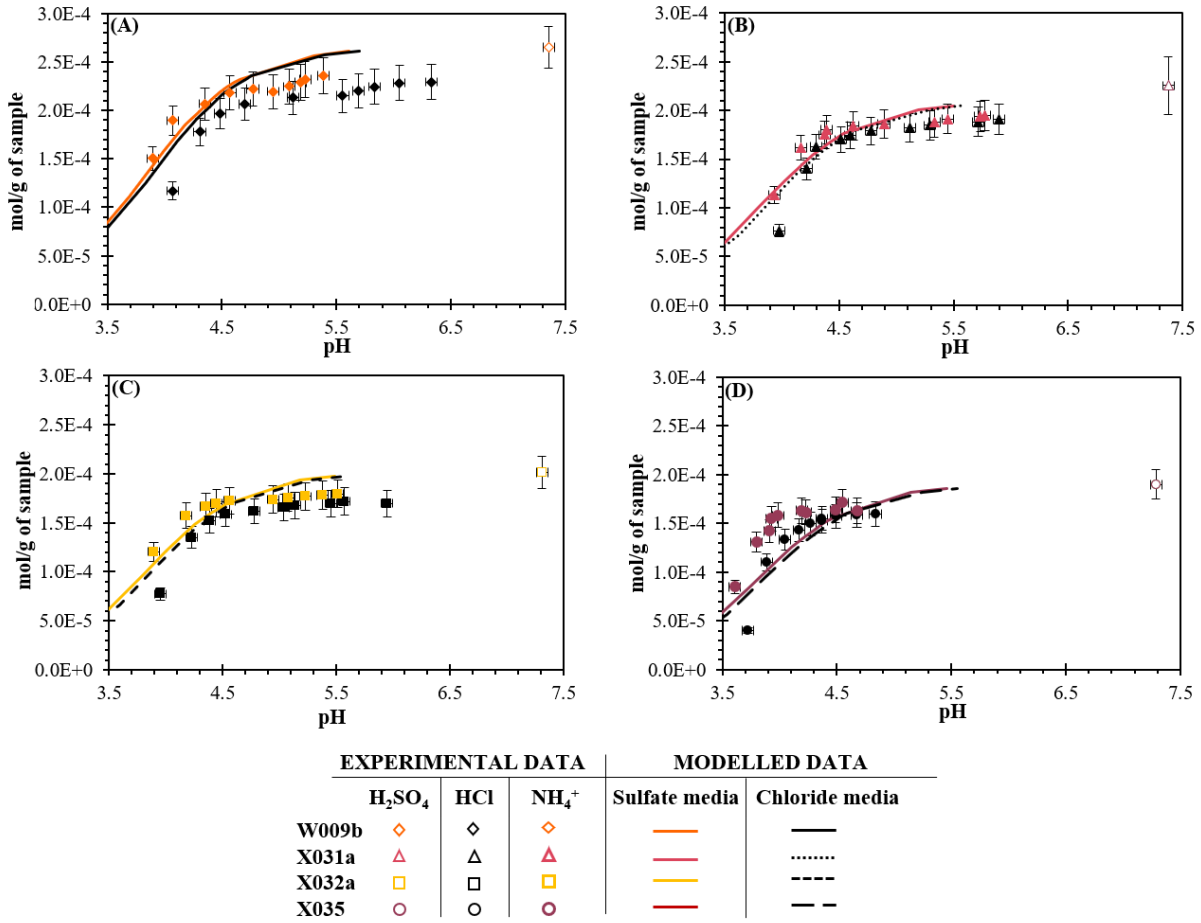

Figure 7: Comparison between the amount of adsorbed Na^+ measured experimentally (calculated from Eq. 1; symbols) and the modeled amount (lines) as a function of pH. Data are reported for chloride $(Na^+/H^+)_{Cl}$ (black symbols)) and sulfate $((Na^+/H^+)_{SO_4}$ (colored symbols) media for 4 Abinky analcimolites ((A) W009b, (B) X031a, (C) X032a, (D) X035). Data as a function of pH are also compared to the amount of Na desorbed with a 1 M NH_4^+ solution at neutral pH (empty symbols; corresponding to CEC_{Na/NH_4} in the text and used as the total site concentration used in the modeling procedure).

609 Since the samples were taken from the same initial solid (see Section 2.2.2.1), it is
610 possible to directly compare the two datasets obtained in chloride and sulfate media for each
611 of the four Abinky analcimolite samples (Fig. 7). For all pH values > 4.5 and for all four
612 samples studied, no difference was observed between the data obtained in both media. Thus,
613 as the main consumers of H^+ are the exchange reactions occurring at the interface between
614 analcime and the solution, as demonstrated earlier, the Na^+ exchange by H^+ is completely
615 independent of the nature of the counter ion (Cl^- or SO_4^{2-}) and depends only on the S/L ratio
616 established in the experiments, *i.e.*, the amount of total exchange sites. However, for
617 experiments with pH < 3.9, the Na_{ads} values for exchange with a sulfate medium are
618 consistently higher than those for a chloride medium. This means that when the sample is in
619 contact with a sulfated solution at pH < 3.9, more Na^+ is adsorbed. This could be explained by
620 a variation in sulfate speciation when the pH varies. Indeed, the distribution of the main forms
621 of aqueous sulfates (SO_4^{2-} and HSO_4^-) in the conditions tested varies between pH values from
622 2 to 3.9, according to previous aqueous calculations performed with PhreeqC.
623
624
625 **3.3.Application to a mining context**
626 *In Situ* Recovering (ISR; IAEA, 2001) is envisaged to recover uranium from the
627 Imouraren deposit in northwestern Niger via the injection of a sulfuric acid solution. The
628 uranium in this deposit is found in the Tchi2 sandstone formation, which contains analcime
629 cement and some analcimolitic levels, and below this, the Abinky formation is composed
630 solely of analcimolites (Fig. S1). The first step in understanding and predicting proton
631 consumption and the mobility of water and solutes in these different geological formations

during acidification is to evaluate the ion-exchange properties of analcime-rich rocks involving H^+.

To assess the consumption of H^+ by Na^+/H^+ ion-exchange reactions occurring with analcime in analcime-rich rocks for "*in situ*" conditions, a calculation simulating the 1D transport of an acid solution in a porous column (thickness of 10 cm) with (i) a porosity of approximately 20% (representative of the analcime-rich rock in geological formations (Billon, 2014)) and (ii) a concentration of ion-exchange sites representative of the analcime content in these rocks was performed. This calculation was inspired by the work of Lu et al. (2014) concerning ion-exchange reactions occurring in soil and sediment columns and was performed by using PhreeqC® software. For this simulation, due to the results discussed in the previous sections, we implicitly assumed that (i) analcime is the only phase able to exchange protons in the analcime-rich rock and that (ii) analcime is stable in these rocks (negligible dissolution), at least when pH > 3.5, allowing us to consider a constant concentration of exchange sites during the simulation. To assess H^+ consumption by Na^+/H^+ reactions, simulations were performed in the presence and absence of Na^+/H^+ ion exchange reactions. When these reactions were considered, the selectivity coefficient proposed in Section 3.2.2.2. (*i.e.*, log $K_{Na/H}$ equal to 1.3) was used, and the ion-exchange site concentration used was calculated by using the CEC_{Na/NH_4} and the porosity (*i.e.*, solid/solution ratio) of the rock. To use conditions representative of the *in situ* conditions, calculations were then performed by using a solid solution ratio equal to 12.5 $kg_{analcime}/L_{water}$, corresponding to a site concentration >Xa (see Section 2.2.2.2.) equal to approximately 2.4 eq/L_{water}. Finally, for the calculation, the initial porosity of the rock (*i.e.*, before the transport of the acid solution) was filled with the pore water of the Tchi2 formation (see chemical composition in Table 2;

electrical balance of the initial pore water was performed with carbonates), and the 1D column was discretized in 50 cells.

Table 2: Simplified composition of the Tchi2 aquifer (Orano, 2023). Concentration values are given in mol/L.

pH	$Al_{(III)}$	C(4)*	Cl^-	K^+	Na^+	$S(6)^{-**}$	Si
9.05	$3.93.10^{-6}$	$3.69.10^{-3}$	$3.10.10^{-4}$	$1.02.10^{-5}$	$4.57.10^{-3}$	$1.55.10^{-4}$	$1.28.10^{-4}$

** correspond to total concentration of dissolved carbonates species*
*** correspond to total concentration of dissolved sulfates species*

Fig. 8 reports the evolution of the pH simulated at the outlet of the column as a function of the number of pore volumes of pH 2 acid solution injected in the column. Data are plotted by considering, or not, Na^+/H^+ ion-exchange reactions and are reported for both chloride and sulfate media.

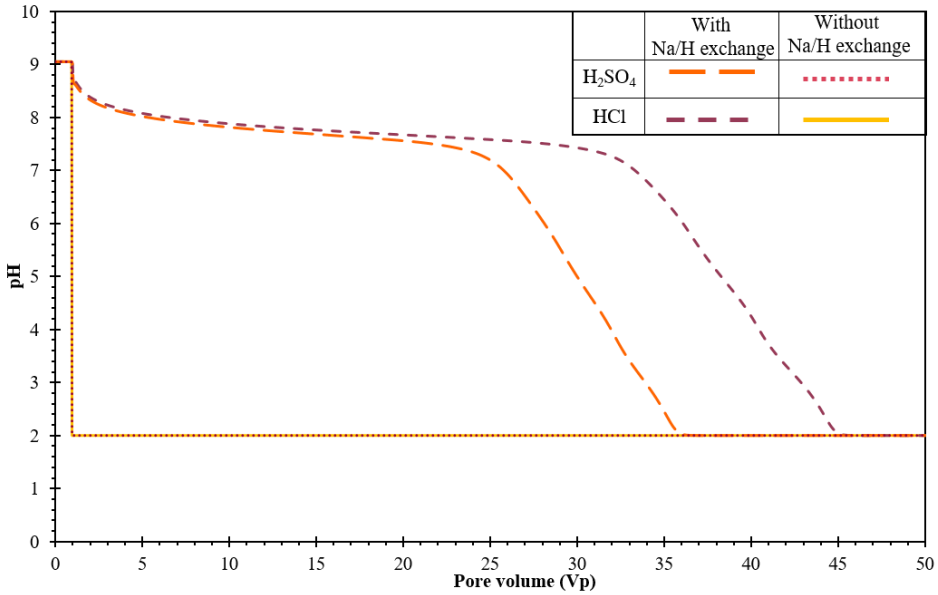

Figure 8: Simulated data reporting the evolution of pH at the outlet of the analcime-rich column as a function of the number of pore volumes percolating through the column following an injection of acid solution (pH=2). Data are plotted in the presence and absence

671 of Na^+/H^+ ion-exchange reactions in HCl and H_2SO_4 solutions. Data are calculated for a rock
672 representative of the X035 rock in term of analcime content and porosity (see text for details).
673
674 In the case in which Na^+/H^+ ion exchange is not considered, the pH evolution is identical
675 for acidification at pH 2 performed with HCl and H_2SO_4 solutions (see Fig. 8). When Na^+/H^+
676 ion exchange is allowed, the pH decrease is strongly attenuated in comparison with conditions
677 in which H^+ is not involved in ion-exchange reactions with Na^+. It should be noted here that
678 the selectivity coefficient was determined for powders in a pH range above 3.5, while the
679 injection solution modeled is intended for a solution at pH 2. Thus, the assumption made is
680 that the behavior of the sample studied will be similar at pH 2 and pH 3.5, assuming that there
681 is no increased dissolution at pH 2 compared to pH 3.5. However, even if dissolution
682 increases at pH 2, H^+ consumption will increase accordingly. In the case of the chloride
683 medium, ~45 Vp is required to obtain an output pH equal to that of the input, whereas ~35 Vp
684 is required in the case of sulfate. This slight difference between these two media can be
685 attributed to a change in sulfate speciation when the pH varies, as mentioned in Section
686 3.2.2.2. Thus, a geological formation such as Abinky composed of analcimolite underlying
687 the host uranium deposit will induce attenuation of the acid plume by proton consumption via
688 Na^+/H^+ exchange reactions occurring between the injected acid solution and the analcimes
689 present in the analcime-rich rock; this effect will be directly linked to the analcime content in
690 the surrounding rock.
691
692
693 **4. Conclusion**

Mineralogical quantification based on Rietveld refinement provides a robust method to determine the proportion of crystalline and amorphous phases in rocks. Through the use of an internal standard, this approach allows refinement of the average structural formula and the quantity of each crystalline mineral phase, recalculating the amount of analcime present in each sample and yielding their total chemical composition. The consistency of these results relative to those from experimental chemistry highlighted the validity of the Rietveld model proposed. The study also reveals that the crystalline chemistry of the obtained analcimes varies very little and is independent of the sample used.

Analysis of the analcime content in relation to the amount of sodium exchanged by the ammonium ion (NH_4^+) for the 37 samples from the four facies of interest highlights a positive correlation between analcime content and exchanged sodium. This correlation is considered to be independent of the structural charge of analcime in the studied samples. Micron-scale powders and a 1 M NH_4^+ solution were used to exchange Na^+, and the results showed that approximately 6.2 ± 1.4% of total sodium is exchanged among the 37 samples, corresponding to a CEC value of approximately 30 meq/100 g (*i.e.*, CEC_{Na/NH_4}) for samples with the highest analcime content (*i.e.*, 85wt% obtained by the Rietveld method).

Experiments conducted with acidic solutions revealed that the main mechanism of proton consumption was ion exchange with Na^+. Given the low chlorite content of the samples and based on measured dissolved magnesium quantities, chlorite dissolution was considered nonsignificant. Thus, the entire measured dissolved silicon content in the supernatants was attributed to analcime dissolution, accounting for less than 0.3wt% of the total dissolution. Therefore, analcime dissolution was considered negligible under the acidic conditions used (pH>3.5), and analcime is considered to have a constant cation exchange capacity in the Na^+/H^+ ion-exchange model proposed. Modeling of the experimental isotherms with ion

exchange occurring at a single site was performed by considering an adsorption site density equal to CEC_{Na/NH_4}. This assumes that NH_4^+ and H^+ ions probe the same amount of Na^+ within the analcime structure. A log $K_{Na/H}$ value of 1.3 was used to interpret all experimental data acquired for the $(Na^+/H^+)_{Cl}$ and $(Na^+/H^+)_{SO4}$ isotherms across the four samples of interest. Thus, as the main consumers of H^+ are the exchange reactions occurring at the interface between analcime and the solution, the amount of exchange of Na^+ by H^+ is completely independent of the nature of the counter ion (Cl^- or SO_4^{2-}) and solely dependent on the solid/solution ratio used in the experiments, *i.e.*, the total quantity of exchange sites. Finally, the results showed that H^+ for Na^+ exchange in analcime plays a major role in the evolution of the pore water pH of an analcime-rich rock subjected to dynamic acidification. Therefore, the Na^+/H^+ reaction should be considered in reactive transport models to simulate the mobilities of ionic solutes in analcime-rich rocks under natural environmental conditions (pH>3.5; room temperature).

Supplementary data (S.D.):

Fig. S1 reports geological information on the Tim Mersoi Basin formations and stratigraphic column of the Cretaceous series. Fig. S2 presents optical microscopy observations under polarized non-analyzed light conditions for the four facies of interest. Fig. S3 presents diffractograms of 4 representative samples of the facies of interest with (i) mineralogical identification, (ii) associated Rietveld refinement and (iii) zoom on angles 12 and 17°2θ (200 and 210 reflection of the analcime). Fig. S4 shows the SEM images of analcime organization and chemical microanalyses (EDS). Fig. S5 presents comparisons of analcime chemistry on the 4 facies of interest.

Acknowledgments

This work was realized with financial support from Orano Mining and supported by the French government program "Investissements d'Avenir" (EUR INTREE, reference ANR-18-EURE-0010). The authors acknowledge financial support from the European Union (ERDF) and Région Nouvelle Aquitaine.

References

Aiello, R., Ming, D., Mumpton, F., 1995. Zeolitic tuffs as building materials in Italy: A review. Natural Zeolites 93, 589–602.

Ames Jr, L., 1966. Cation exchange properties of wairakite and analcime. American Mineralogist: Journal of Earth and Planetary Materials 51, 903–909. http://www.minsocam.org/ammin/AM51/AM51_903.pdf

Armbruster, T., Gunter, M.E., 2001. Crystal structures of natural zeolites. Reviews in mineralogy and geochemistry 45, 1–67. https://doi.org/10.2138/rmg.2001.45.1

Atta, A., Jibril, B., Aderemi, B., Adefila, S., 2012. Preparation of analcime from local kaolin and rice husk ash. Applied Clay Science 61, 8–13. https://doi.org/10.1016/j.clay.2012.02.018

Azizi, S.N., Yousefpour, M., 2011. Isomorphous substitution of iron and nickel into analcime zeolite. Zeitschrift für Anorganische und Allgemeine Chemie (ZAAC) - Journal of inorganic and general chemistry. https://doi.org/10.1002/zaac.201100059

Bailey, S., 1969. Refinement of an intermediate microcline structure. American Mineralogist: Journal of Earth and Planetary Materials 54, 1540–1545.

Bargar, K.E., Beeson, M.H., 1985. Hydrothermal alteration in research drill hole Y-3, Lower Geyser Basin, Yellowstone National Park, Wyoming. https://doi.org/10.3133/pp1054C

Barrante, J. R. (1974). Applied Mathematics for Physical Chemistry

Barrer, R., Hinds, L., 1953. 386. Ion-exchange in crystals of analcite and leucite. Journal of the Chemical Society (Resumed) 1879–1888. https://doi.org/doi:10.1039/jr9530001879

Barrer, R.M., 1981. Zeolites and their synthesis. Zeolites 1, 130–140. https://doi.org/10.1016/S0144-2449(81)80001-2

Bergmann, J., Kleeberg, R., 1998. Rietveld analysis of disordered layer silicates. Presented at the Materials Science Forum, Trans Tech Publ, pp. 300–305. https://doi.org/10.4028/www.scientific.net/MSF.278-281.300

Billon, S., 2014. Minéraux argileux dans le gisement uranifère d'Imouraren (Bassin de Tim Mersoï, Niger): Implications sur la genèse du gisement et sur l'optimisation des processus de traitement du minerai. PhD, Poitiers, France. https://www.theses.fr/2014POIT2263

Billon, S., Patrier, P., 2019. Diagenetic and hydrothermal history of the host rock of the Imouraren uranium deposit (Tchirezrine 2 Formation-Tim Mersoï Basin, Niger). Journal of African Earth Sciences 160, 103637. https://doi.org/10.1016/j.jafrearsci.2019.103637

Blanc, P., Lassin, A., Piantone, P., Azaroual, M., Jacquemet, N., Fabbri, A., Gaucher, E.C., 2012. Thermoddem: A geochemical database focused on low temperature water/rock interactions and waste materials. Applied geochemistry 27, 2107–2116. https://doi.org/10.1016/j.apgeochem.2012.06.002

Broxton, D.E., Bish, D.L., Warren, R.G., 1987. Distribution and chemistry of diagenetic minerals at Yucca Mountain, Nye County, Nevada. Clays and Clay Minerals 35, 89–110. https://doi.org/10.1346/CCMN.1987.0350202

Calleri, M., Ferraris, G., 1964. Struttura dell'analcime: $Na\text{-}AlSi_2O_6.H_2O$. Atti dell'Accademia delle Scienze di Torino 98, 821–846.

Chipera, S.J., Bish, D.L., 2010. Rehydration kinetics of a natural analcime. European Journal of Mineralogy 22, 787–795. https://doi.org/10.1127/0935-1221/2010/0022-2036

Clifton, R.A., 1987. Natural and synthetic zeolites. Crystals 10 Issue 7.

Colella, C., Gennaro, M. de', Aiello, R., 2001. Use of zeolitic tuff in the building industry. Reviews in mineralogy and geochemistry 45, 551–587. https://doi.org/10.2138/rmg.2001.45.16

Coombs, D.S., 1955. X-ray observations on wairakite and non-cubic analcime. Mineralogical magazine and journal of the Mineralogical Society 30, 699–708. https://doi.org/10.1180/minmag.1955.030.230.03

De Boissezon, H., Levy, L., Jakymiw, C., Distinguin, M., Guerin, F., Descostes, M., 2020. Modeling uranium and ^{226}Ra mobility during and after an acidic in situ recovery test (Dulaan Uul, Mongolia). Journal of Contaminant Hydrology 235, 103711. https://doi.org/10.1016/j.jconhyd.2020.103711

Deer, Howie, Zussman, 2004. Framework Silicates: Silica Minerals, Feldspathoids and the Zeolites. Second Edition, The Geological Society. ed, Rock-Forming Mineral. https://doi.org/10.1017/S0016756806312484

Defang, H., Nikishov, A., 2009. Effect of dietary inclusion of zeolite on performance and carcass quality of grower-finisher pigs. Energy (ME) 47, 43–9. https://www.lrrd.cipav.org.co/lrrd21/6/defa21090.htm

Doebelin, N., Kleeberg, R., 2015. Profex: a graphical user interface for the Rietveld refinement program BGMN. Journal of applied crystallography 48, 1573–1580. https://doi.org/10.1107/S1600576715014685

Dyer, A., Tangkawanit, S., Rangsriwatananon, K., 2004. Exchange diffusion of Cu^{2+}, Ni^{2+}, Pb^{2+} and Zn^{2+} into analcime synthesized from perlite. Microporous and mesoporous materials 75, 273–279. https://doi.org/10.1016/j.micromeso.2004.07.007

English, P., 2001. Formation of analcime and moganite at Lake Lewis, central Australia: significance of groundwater evolution in diagenesis. Sedimentary Geology 143, 219–244. https://www.osti.gov/etdeweb/biblio/22444085

Escario, S., Seigneur, N., Collet, A., Regnault, O., de Boissezon, H., Lagneau, V., Descostes, M., 2023. A reactive transport model designed to predict the environmental footprint of an 'in-situ recovery' uranium exploitation. Journal of Contaminant Hydrology 254, 104106. https://doi.org/10.1016/j.jconhyd.2022.104106

Eyde, T., 1993. Using Zeolite in the Recovery of Heavy Metals From Mining Effluents. Presented at the EPD Congress 1993, pp. 383–392.

Ferraris, G., Jones, D., Terkess, J., 1972. A neutron-diffraction study of the crystal structure of analcime, $NaAlSi_2O_6 \cdot H_2O$. Zeitschrift für Kristallographie-Crystalline Materials 135, 240–483. https://doi.org/10.1524/zkri.1972.135.16.240

Gall, Q., Hyde, R., 1989. Analcime in lake and lake- margin sediments of the Carboniferous Rocky Brook Formation, Western Newfoundland, Canada. Sedimentology 36, 875–887. https://doi.org/10.1111/j.1365-3091.1989.tb01751.x

Ion exchange in mordenite. Verification of the triangle rule. Journal of Chemical and Engineering Data 26, 366–367. https://doi.org/10.1021/je00026a005

Harada, K., Iwamoto, S., Kihara, K., 1967. Erionite, phillipsite and gonnardite in the amygdales of altered basalt from Maze, Niigata Prefecture, Japan. American Mineralogist: Journal of Earth and Planetary Materials 52, 1785–1794. http://www.minsocam.org/ammin/AM52/AM52_1785.pdf

Harada, K., Nagashima, K., 1972. New data on the analcime—wairakite series. American Mineralogist: Journal of Earth and Planetary Materials 57, 924–931.

Harlow, G.E., 1982. The anorthoclase structures: the effects of temperature and composition. American Mineralogist 67, 975–996. http://www.minsocam.org/ammin/AM67/AM67_975.pdf

Hay, R.L., 1970. Silicate reactions in three lithofacies of a semi-arid basin, Olduvai Gorge, Tanzania. Mineralogical Society of America Special Paper 3, 237–255. https://msaweb.org/wp-content/uploads/2022/07/MSA_SP3_237-256.pdf

Hayhurst, D., 1978. The potential use of natural zeolites for ammonia removal during coal-gasification. Natural Zeolites. Occurrence, Properties and Use 503–8.

Hazen, R.M., Finger, L.W., 1979. Polyhedral tilting: a common type of pure displacive phase transition and its relationship to analcite at high pressure. Phase Transitions: A Multinational Journal 1, 1–22. https://doi.org/10.1080/01411597908213181

High, L.R., Picard, M.D., 1965. Sedimentary petrology and origin of analcime-rich Pogo Agie Member, Chugwater (Triassic) Formation, west-central Wyoming. Journal of Sedimentary Research 35, 49–70. https://doi.org/10.1306/74D711EF-2B21-11D7-8648000102C1865D

IAEA, 2001. International Atomic Energy Agency, 2001. Manual of Acid in Situ Leach Uranium Mining Technology.

Johnson, G., Flotow, H., O'hare, P., 1982. Thermodynamic studies of zeolites: analcime and dehydrated analcime. American Mineralogist 67, 736–748. http://www.minsocam.org/ammin/AM67/AM67_736.pdf

Jones, R., Babcock, C., Knowlton, W., 2000. Estimation of the total amorphous content of Hawai'I soils by the Rietveld Method. Soil Science Society of America Journal 64, 1100–1108. https://doi.org/10.2136/sssaj2000.6431100x

Joulia, F., Bonifas, M., Weil, R., Camez, T., Millot, G., 1958. Analcimolites sédimentaires dans le Continental Intercalaire du Sahara central (Bassin du Niger, AO F). Sciences Géologiques, bulletins et mémoires 11, 67–70. https://www.persee.fr/doc/sgeol_0037-2560_1958_num_11_2_1190

Kalita, A., Chelishchev, N., 1995. Use of zeolite containing rocks for water purification. Razved Okhr Nedr 7, 19–20.

Kalló, D., 2001. Applications of natural zeolites in water and wastewater treatment. Reviews in mineralogy and geochemistry 45, 519–550. https://doi.org/10.2138/rmg.2001.45.15

Karlsson, H.R., Clayton, R.N., 1991. Analcime phenocrysts in igneous rocks: primary or secondary? American Mineralogist 76, 189–199. http://www.minsocam.org/ammin/AM76/AM76_189.pdf

Klug, H.P., Alexander, L.E., 1954. X-ray diffraction procedures. Wiley, New-York.

Knight, A., 1960. Residual Aluminum: Its Estimation and Control. Proc. Society Water Treatment and Exam 9, 72.

878 Knowles, C., Rinaldi, F., Smith, J., 1965. Refinement of the crystal structure of analcime.
879 Indian Mineralogist 6, 127–140.
880 Komarneni, S., Roy, R., 1981. Zeolites for fixation of cesium and strontium from radwastes
881 by thermal and hydrothermal treatments. Nuclear and Chemical Waste Management 2,
882 259–264. https://doi.org/10.1016/0191-815X(81)90052-8
883 Kotsis, L., Argyelán, J., Szolcsányi, P., Pataki, K., 1982. Application of natural zeolites for air
884 separation. Reaction Kinetics and Catalysis Letters 18, 149–153.
885 https://doi.org/10.1007/BF02065154
886 Lagneau, V., Regnault, O., Descostes, M., 2019. Industrial deployment of reactive transport
887 simulation: An application to uranium in situ recovery. Reviews in Mineralogy and
888 Geochemistry 85, 499–528. https://doi.org/10.2138/rmg.2019.85.16 Line, C., Winkler,
889 B., Dove, M., 1994. Quasielastic incoherent neutron scattering study of the rotational
890 dynamics of the water molecules in analcime. Physics and Chemistry of Minerals 21,
891 451–459. https://doi.org/10.1007/BF00202275
892 Lu, J., Tertre, E., Beaucaire, C., 2014. Assessment of a predictive model to describe the
893 migration of major inorganic cations in a Bt soil horizon. Applied geochemistry 41,
894 151–162. https://doi.org/10.1016/j.apgeochem.2013.12.009
895 Luhr, J.F., Kyser, T.K., 1989. Primary igneous analcime: The Colima minettes. American
896 Mineralogist 74, 216–223. http://www.minsocam.org/ammin/AM74/AM74_216.pdf
897 Madsen, I., Scarlett, N., Kleeberg, R., Knorr, K., 2019. Quantification of phases with partial
898 or no known crystal structures. https://doi.org/10.1107/97809553602060000954
899 Mallah, M.H., Soorchi, H., Jooybari, T.F., 2012. Development of empirical equation for
900 analcime in the treatment of nuclear waste. Annals of Nuclear Energy 47, 140–145.
901 https://doi.org/10.1016/j.anucene.2012.04.015
902 Markgraf, S.A., Reeder, R.J., 1985. High-temperature structure refinements of calcite and
903 magnesite. American Mineralogist 70, 590–600.
904 http://www.minsocam.org/ammin/AM70/AM70_590.pdf
905 Mazzi, F., Galli, E., 1978. Is each analcime different? American Mineralogist 63, 448–460.
906 http://www.minsocam.org/ammin/AM63/AM63_448.pdf
907 Mercer, B., Ames, L., 1978. Zeolite ion exchange in radioactive and municipal wastewater
908 treatment. Natural zeolites; occurrence, properties and uses 25, 451–462.
909 Millot, 1963. Géologie des argiles. Masson & Cie, Paris.
910 Mimura, H., Tezuka, T., Akiba, K., 1995. Formation of analcime film under hydrothermal
911 conditions. Journal of nuclear science and technology 32, 1250–1258.
912 https://doi.org/10.3327/jnst.32.1250
913 Ming, D.W., Allen, E.R., 2001. 18. Use of Natural Zeolites in Agronomy, Horticulture and
914 Environmental Soil Remediation, in: Natural Zeolites. De Gruyter, pp. 619–654.
915 https://doi.org/10.1515/9781501509117-020
916 Ming, D.W., Boettinger, J.L., 2001. Zeolites in soil environments. Reviews in mineralogy and
917 geochemistry 45, 323–345. https://doi.org/10.2138/rmg.2001.45.11
918 Ming, D.W., Mumpton, F.A., 1989. Zeolites in soils. Minerals in soil environments 1, 873–
919 911. https://doi.org/10.2138/rmg.2001.45.11
920 Mondale, K., Carland, R., Aplan, F., 1995. The comparative ion exchange capacities of
921 natural sedimentary and synthetic zeolites. Minerals Engineering 8, 535–548.
922 https://doi.org/10.1016/0892-6875(95)00015-I
923 Montalvo, S., Guerrero, L., Borja, R., Sánchez, E., Milán, Z., Cortés, I., De La La Rubia,
924 M.A., 2012. Application of natural zeolites in anaerobic digestion processes: A
925 review. Applied Clay Science 58, 125–133. https://doi.org/10.1016/j.clay.2012.01.013

Pacquet, A., 1968. Analcime et argiles diagénétiques dans les formations sédimentaires de la région d'Agadès (République du Niger). Persée-Portail des revues scientifiques en SHS.

Parkhurst, D.L., Appelo, C., 1999. User's guide to PHREEQC (Version 2): A computer program for speciation, batch-reaction, one-dimensional transport, and inverse geochemical calculations. Water-resources investigations report 99, 312.

Pechar F, n.d. Crystal-chemistry of analcime. Acta Univ Carol Geol 1989; 4: 469-487.

Pesonen, J., Tuomikoski, S., Näppä, J., Prokkola, H., Hu, T., Lassi, U., Runtti, H., 2021. Ammonium Uptake over Analcime and Its Soil Enhancer Potential. Presented at the Proceedings of the 8th International Conference on Sustainable Solid Waste Management, Thessaloniki, Greece, pp. 23–26.

Pond, W., Laurent, S., Orloff, H., 1984. Effect of dietary clinoptilolite or zeolite Na-A on body weight gain and feed ulilization of growing lambs fed urea or intact protein as a nitrogen supplement. Zeolites 4, 127–132. https://doi.org/10.1016/0144-2449(84)90050-2

Ratterman, N.G., Surdam, R.C., 1981. Zeolite mineral reactions in a tuff in the Laney Member of the Green River Formation, Wyoming. Clays and Clay Minerals 29, 365–377. https://doi.org/10.1346/CCMN.1981.0290506

Remy, R.R., Ferrell, R.E., 1989. Distribution and origin of analcime in marginal lacustrine mudstones of the Green River Formation, south-central Uinta Basin, Utah. Clays and Clay minerals 37, 419–432. https://doi.org/10.1346/CCMN.1989.0370505

Renaut, R., 1993. Zeolitic diagenesis of late Quaternary fluviolacustrine sediments and associated calcrete formation in the Lake Bogoria Basin, Kenya Rift Valley. Sedimentology 40, 271–301. https://doi.org/10.1111/j.1365-3091.1993.tb01764.x

Rietveld, H.M., 1969. A profile refinement method for nuclear and magnetic structures. Journal of applied Crystallography 2, 65–71. https://doi.org/10.1107/S0021889869006558

Sakirci, M., 2016. Investigation of thermal and structural properties of natural and ion-exchanged analcime. Anadolu University Journal of Science and Technology A-Applied Sciences and Engineering 17, 724–734. https://doi.org/10.18038/aubtda.266863

Seki, Y., Oki, Y., 1969. Wairakite-analcime solid solutions from low-grade metamorphic rocks of the Tanzawa Mountains, Central Japan. Mineralogical Journal 6, 36–45. https://www.jstage.jst.go.jp/article/minerj1953/6/1-2/6_1-2_36/_pdf

Semmens, M., Seyfarth, M., 1978. The Selectivity of Clinoptilolite for Heavy Metals. Presented at the Proceedings of the Ziolite 76 Conference.

Sheppard, R.A., Gude, A.J., 1973. Zeolites and associated authigenic silicate minerals in tuffaceous rocks of the Big Sandy Formation, Mohave County, Arizona. https://doi.org/10.3133/pp830

Shull, K.E., Guthan, G.R., 1967. Rapid modified eriochrome cyanine R method for determination of aluminum in water. Journal- American Water Works Association 59, 1456–1468. https://doi.org/10.1002/j.1551-8833.1967.tb03476.x

Strickland, J.D.H., Parsons, T.R., 1972. A practical handbook of seawater analysis.

Tang, Z., Parnell, J., Longstaffe, F.J., 1997. Diagenesis of analcime-bearing reservoir sandstones; the Upper Permian Pingdiquan Formation, Junggar Basin, Northwest China. Journal of Sedimentary Research 67, 486–498. https://doi.org/10.1306/D42685A4-2B26-11D7-8648000102C1865D

Taylor, W., 1930. I. The structure of analcite ($NaAlSi_2O_6 \cdot H_2O$. Zeitschrift für Kristallographie-Crystalline Materials 74, 1–19. https://doi.org/10.1524/zkri.1930.74.1.1

Toby, B.H., 2006. R factors in Rietveld analysis: How good is good enough? Powder diffraction 21, 67–70. https://doi.org/10.1154/1.2179804

Tsitsishvili, V., Dolaberidze, N., Mirdzveli, N., Nijaradze, M., Amiridze, Z., 2020. Properties of bactericidal adsorbents prepared from Georgian natural analcime and phillipsite. Bull. Georgian Natl. Acad. Sci 14, 25–33

Underdown, D., Hickey, J., Kalra, S., 1990. Acidization of analcime-cemented sandstone, Gulf of Mexico. Presented at the SPE Annual Technical Conference and Exhibition, OnePetro. https://doi.org/10.2118/20624-MS

Valsardieu, 1971. Etude géologique et paléogéographique du bassin de Tim Mersoï - Région d'Agadès (République du Niger). https://www.persee.fr/doc/sgeol_0037-2560_1971_num_24_4_1396

Vanderstappen, R., Verbeek, T., 1959. Présence d'analcime d'origine sédimentaire dans le Mésozoïque du bassin du Congo. Bulletin de la Société Belge de Géologie 68, 417–421.

Wagani, I., 2007. Potentialités uranifères des sources volcaniques envisageables pour la formation des minéralisations de la région d'Arlit (Niger). https://www.theses.fr/2007PA112004

Walton, A.W., 1975. Zeolitic diagenesis in Oligocene volcanic sediments, Trans-Pecos Texas. Geological Society of America Bulletin 86, 615–624. https://doi.org/10.1130/0016-7606(1975)86<615:ZDIOVS>2.0.CO;2

Wang, J., Liang, C., Cao, Y., Tian, Y., 2022. Occurrence, Genesis, and Significance of Analcime in Fine-Grained Sedimentary Rocks. Geofluids 2022. https://doi.org/10.1155/2022/3633047

Westphal, T., Füllmann, T., Pöllmann, H., 2009. Rietveld quantification of amorphous portions with an internal standard—Mathematical consequences of the experimental approach. Powder Diffraction 24, 239–243. https://doi.org/10.1154/1.3187828

Wilkin, R., Barnes, H., 1998. Solubility and stability of zeolites in aqueous solution; I, Analcime, Na-, and K-clinoptilolite. American Mineralogist 83, 746–761. https://doi.org/10.2138/am-1998-7-807

Wilkinson, J., Hensel, H., 1994. Nephelines and analcimes in some alkaline igneous rocks. Contributions to Mineralogy and Petrology 118, 79–91. https://doi.org/10.1007/BF00310612

Wilkinson, J., Whetten, J., 1964. Some analcime-bearing pyroclastic and sedimentary rocks from New South Wales. Journal of Sedimentary Research 34, 543–553. https://doi.org/10.1306/74D710E6-2B21-11D7-8648000102C1865D

Wise, W.S., Kleck, W.D., 1988. Sodic clay-zeolite assemblage in basalt at Boron, California. Clays and Clay Minerals 36, 131–136. https://doi.org/10.1346/CCMN.1988.0360205

Yoder Jr, H., Weir, C., 1960. High-pressure form of analcite and free energy change with pressure of analcite reactions. American Journal of Science 258, 420–433. https://doi.org/10.1016/j.marpetgeo.2019.104164

Zhu, S., Cui, H., Jia, Y., Zhu, X., Tong, H., Ma, L., 2020. Occurrence, composition, and origin of analcime in sedimentary rocks of non-marine petroliferous basins in China. Marine and Petroleum Geology 113, 104164. https://doi.org/10.1016/j.marpetgeo.2019.104164